Materials Development for Construction of Deep Underground Tunnels and Structures

Minoru INADA*[1]   Kazuyuki TAZAKI*[1]
Munehiro ISHIDA*[1]   Youichi SANO*[1]
Kenichirou IMAFUKU*[2]

Abstract

The development of key technologies to enable the use of deep underground space is significant for effective utilization of Japan's limited building area and for providing infrastructures in overpopulated urban districts. To construct large-scale underground structures at great depths safely and effectively, high-quality, high-strength construction materials are indispensable. Nippon Steel Corporation aims to develop high-quality steel products to reduce overall construction costs of deep underground structures and subsequently to promote the effective use of deep underground space. This paper introduces some new technologies we have developed; such as steel diaphragm walls (NS-BOX), primary lining system of steel segments (Concrete Packed Steel Segments) and joint members for highly functional reinforced concrete segments (High Stiffness Joints for Segments).

1. Introduction

In November 1997, the Japanese Government proclaimed its Emergent Economic Policy Package for Reforming Japan for the 21st Century. The program includes reforming the economic structure, activating land transactions, making effective use of land, and creating an attractive business environment through deregulation. Promoting the use of underground space in urban areas was positioned as a critical policy issue under the program. The Action Plan for Economic Structural Reform and Creation in May 1997 points to the necessity of deep underground space development technology for urban environmental improvement as one of 15 areas expected to grow in the future. The Provisional Investigation Committee for Deep Subterranean Utilization, established within the government, examined and discussed the definition, technology, safety, and environment of deep underground space in legal and other associated terms. The committee issued its final report on the utilization of deep underground space in May 1998.

Nippon Steel's Structural Group conceptualized an overall system of underground space construction material development and organized such materials into two major types: materials for plane structures like shafts and basements, and materials for line structures like tunnels. The Structurals Group is now developing underground space construction materials that incorporate a wide spectrum of steel technology to create new applications for steel products.

The NS-BOX is a plane underground structure construction material for use in the construction of shafts and deep underground space walls at confined sites. The development of line underground structure construction materials focuses on shield tunnel linings. Our research and development of steel segments aims to meet various needs, including use at great underground depths, inner water pressure, and non-circular cross sections. High-stiffness joint fasteners to be used for not only steel segments but also reinforced-concrete (RC) segments are also being developed. Large-section space construction methods for road tunnels and other underground structures are under research and development, as well. The Structurals Group is establishing a system to further promote these

---

*[1] Construction & Architectural Materials Development & Engineering Sevice Division

*[2] Technical Development Bureau

developments.

This report describes the development of three product technologies: NS-BOX, concrete-packed (CP) steel segments, and high-stiffness joints.
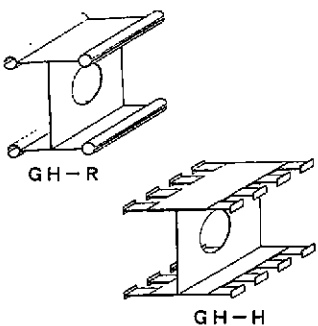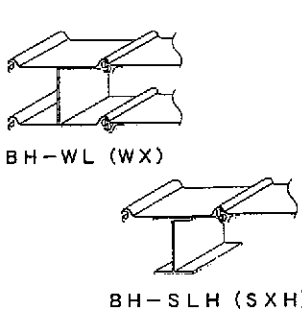
2. Steel Diaphragm Wall Method

2.1 Overview

Steel sheet piles and steel pipe sheet piles have been traditionally used for earth retaining walls, but steel members that could be used to build earth retaining walls 30 to 100 m deep in urban areas were not available. Steel sheet piles with high stiffness and strength are also in demand for thinner earth retaining walls within maximum depth of 30 m. Nippon Steel has developed its GH type NS-BOX for great-depth earth retaining walls and its BH type NS-BOX with higher stiffness than that of steel sheet piles for small- and medium-depth earth retaining walls. The GH and BH of NS-BOX types and the types of earth retaining walls by depth are shown in **Table 1**, **Fig. 1**, and **Photos 1 to 3**. The NS-BOX series features reduced wall thickness, site space saving, and prefabrication. The GH type is filled with concrete as shown in **Fig. 2** and is different from

Product and method	Steel sheetpile	Steel pipe sheetpile	NS-BOX BH	NS-BOX GH	Soil mixing wall	RC diaphragm wall
Demand in cities	○	△	◎	◎	◎	◎
Demand in harbors and rivers	◎	◎	◎	△	△	△

Applicable depth							
10m						
20m						
30m						
40m						
50m						
60m						
70m – 100m						

Fig. 1 Types of earth retaining walls by depth

Table 1 General data of GH and BH types NS-BOX

| Product	NS-BOX (GH)	NS-BOX (BH)
Structure	G H – R / G H – H	B H – W L (W X) / B H – S L H (S X H)
Properties	• Reduced wall thickness • Site space saving • Saved lavor input, shortened work	• High stiffness • Reduced wall thickness • Site space saving
Application	1) Sub-way tunnels 2) Underground road 3) Shafts 4) Water treatment 5) Underground parking	1) Protection of rever wall 2) Earth retaining wall 3) Shafts (High stiffness specification of sheet pile)
Method	Drilling	• Hammering • pressing
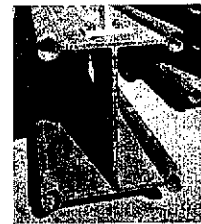
Photo 1 GH-R type NS-BOX
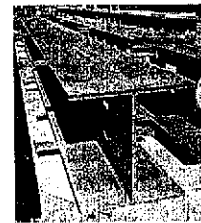
Photo 2 GH-H type NS-BOX

Photo 3 BH-WL type NS-BOX
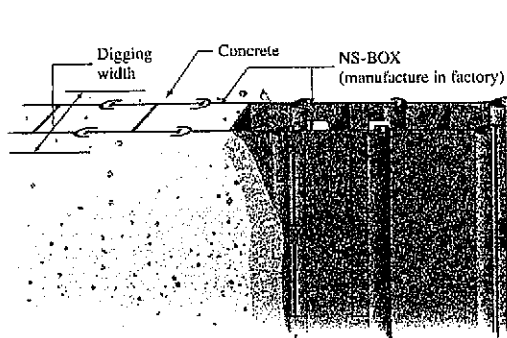
Steel diaphragm wall
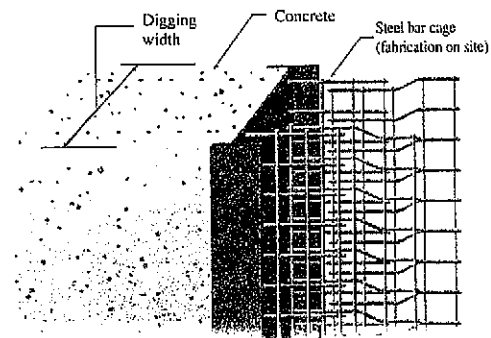
Conventional concrete diaphragm wall

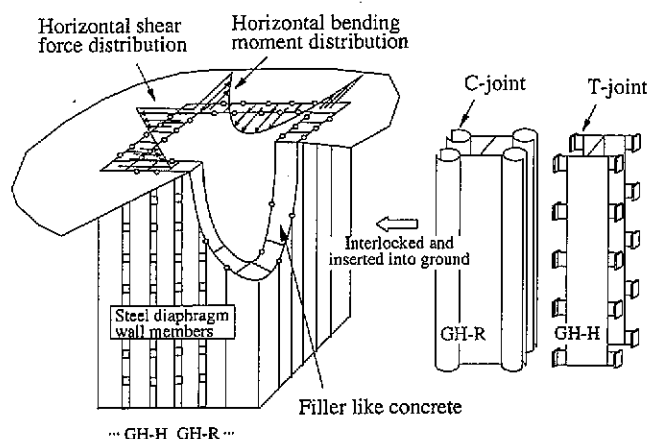Fig. 2 Schematic illustration of diaphragm walls

Fig. 3 Schematic illustration of rectangular shaft

Fig. 5 Load–displacement curves

Table 2 Typical test specimen data and test results

Specimen	Pipe wall thickness (mm)	C-joint strength (N/mm²)	T-joint end width (mm)	Mortar compressive strength (N/mm²)	Interlocking condition	Tensile capacity (kN)
Case 1	12	403	58	25	Neutral	161
Case 2	16	406	58	32	Neutral	213
Case 3	12	403	68	32	Neutral	201
Case 4	16	406	68	32	Neutral	343

conventional steel retaining walls in that it can be utilized as permanent underground walls. The following section describes the development of a two-way slab structure with respect to the horizontal bending moment and shearing force (see **Fig. 3**) required for rectangular shafts using the GH type.

2.2 Development of two-way slab structure
2.2.1 Confirmation of interlocking joint tensile performance

The interlocking joints of steel diaphragm walls consist of pipe-shaped C-joints and T-shaped T-joints that are connected by the filled concrete. The interlocking joints are steel-concrete composite structural members that transmit horizontal stress. To identify the tensile characteristics of the interlocking joints, their full-size specimens were tested under tensile force as shown in **Fig. 4**. The joint parameters were the C-joint pipe wall thickness (t_p), T-joint end width (b), interlocking condition, C-joint material strength (f_y), and filling mortar strength (f_c). The load, interlocking joint relative displacement, and steel strain were measured.

The load–displacement curves are shown in **Fig. 5**, the tensile test specimen data and tensile test results are listed in **Table 2**, and interlocking joint failures are shown in **Fig. 6**. As the load was increased, cracked cross section formed in the filled mortar. The combined action of tensile force and bending moment through the filled mortar makes the C-joint pipe yield. The T-joint sprang out of the C-joint upon reaching its ultimate state. Assuming that the tensile capacity (P_u) of interlocking joints is proportional to the square of t_p and to f_y, the joint capacity of the interlocking joints was determined by regression calculations from the joint tension test results. The design capacity of the interlocking joints are given
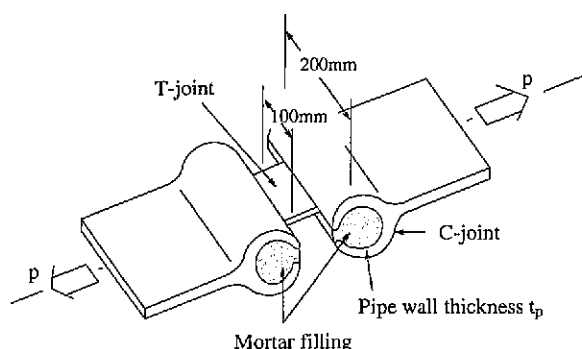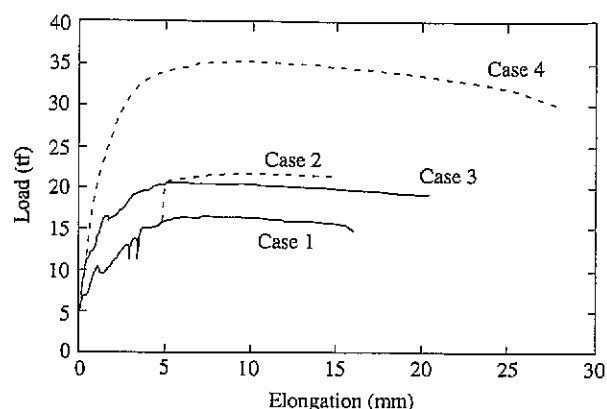

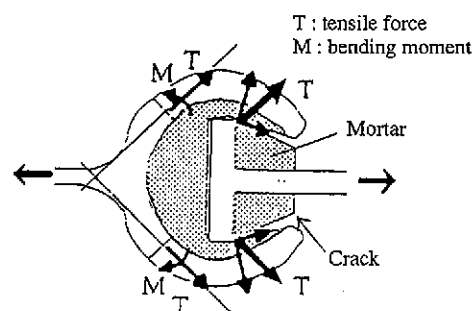Fig. 6 Failure of interlocking joint

Table 3 Design capacity of interlocking joints (kN per joint)

C-joint		Allowable tensile force			
Pipe wall thickness	Grade	Without C-joint reinforcement		With C-joint reinforcement*	
		T-joint A	T-joint B	T-joint A	T-joint B
12	SS400	31.4	44.1	61.8	82.4
	SM490	42.2	59.8	82.4	110
16	SS400	55.9	79.5	109	146
	SM490	74.6	106	132	206
19	SS400	78.5	112	132	206
	SM490	105	149	132	207

* C-joint reinforcement consists of hexagonal steel bars installed inside of C-joint at end
Types A and B of T-joints are used.

Fig. 4 Tension test of interlocking joint

in **Table 3**. The allowable tensile capacity of the interlocking joints were set at one-third of the regression-calculated values. Some interlocking joints were reinforced with hexagonal steel bars. Since

tensile strength changes with the interlocking condition during construction, the allowable tebsile capacity of the reinforced interlocking joint was set to have 10% of allowance to the deviation of interlocking condition.

2.2.2 Confirmation of horizontal bending performance and establishment of design method for bending

To study the capacity of steel diaphragm wall incorporating interlocking joints under the horizontal out-of-plane bending moment, beam members with interlocking joints in the pure bending section were tested where the beam is simply supported and loaded at two intermediaste points. Load, deflection, and steel and concrete strains were measured. The specimens are illustrated in **Fig. 7**, and the principal stresses in the concrete are shown in **Fig. 8**. The principal stress distribution of the concrete cross section at the interlocking joint was such that a rectangular stress block formed in the compression zone of the section. A stress distribution like that of a reinforced-concrete member was observed. The tensile force–elongation relationship of the interlocking joints are shown in **Fig. 9**, and the tensile force–strain relationship of the interlocking joints are shown in **Fig. 10**. The tensile force–elongation relationship and the tensile force–strain relationship of the interlocking joints in tension zone well agree with the tensile test results of the interlocking joints. The load–displacement curves are shown in **Fig. 11**, and the tension test results are listed in **Table 4**. The maximum bending capacity can be calculated conservatively by formulae for RC member with tension reinforcement only that are converted in
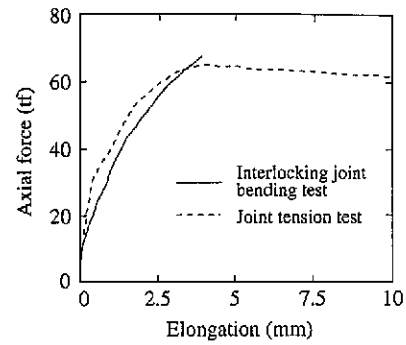
Fig. 9 Relationship between axial force and elongation of interlocking joints
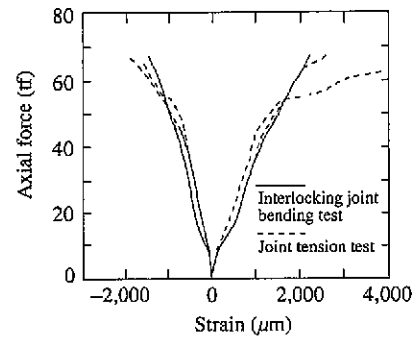
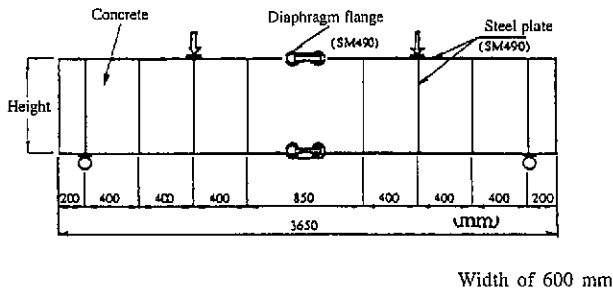Fig. 10 Relationship between axial force and strain of interlocking joints

Width of 600 mm
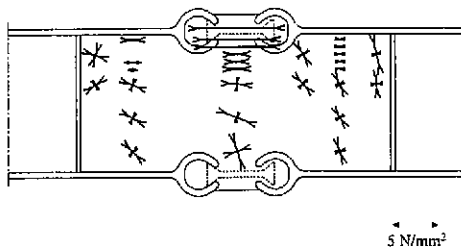
Fig. 7 Schematic illustration of specimens M-1 and M-2

5 N/mm²

Fig. 8 Principal stress in concrete (M-1: P = 561 kN)

Center deflection (mm)
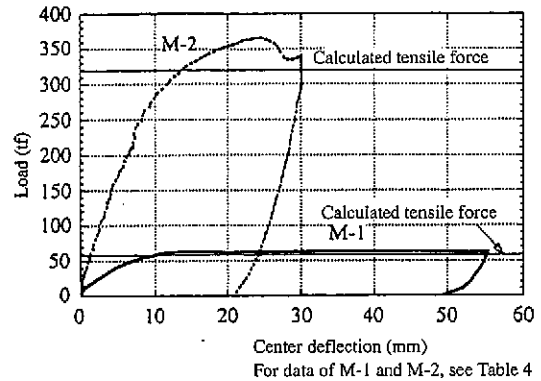For data of M-1 and M-2, see Table 4

Fig. 11 Load–deflection curves

proportion to the capacity of interlocking jouints. Here, the effective cross-sectional area of the interlocking joint in tension is calculated by the following formula:

$$A_s = T_a / f_{sa}$$

where,

Table 4 Test results

Test case	Flange thickness (mm)	Depth of beam (mm)	Joint tensile strength T_{um}(kN/m)	Concrete compressive strength f_c(N/mm²)	test Pu[1] (kN)	calPu1[2] (kN)	calPu2[3] (kN)	testPu / calPu1	testPu / calPu2
M-1	16	400	1,055	21	624	574	633	1.09	0.99
M-2	12	700	3,188	28	3,600	3,139	3,345	1.15	1.08

[1] testPu: Maximum test load, [2] calPu1: Calculated tensile force for single-reinforcement RC member, [3] calPu2: Calculated tensile force for steel member

For M-1 joint, t_p = 16 (SM490) and T-joint A was used. For M-2 joint, t_p = 16 (SM490), and T-joint B and hexagonal steel bars reinforcement were used (see **Table 3**).

A_s: Effective cross-sectional area of interlocking joint with equivalent tensile capacity (mm^2)

T_a: Allowable tensile capacity of interlocking joint (N)

f_{sa}: Allowable tensile stress of steel comosing C-joint (N/mm^2)

The relationship between the bending moment and the curvature is shown in **Fig. 12**. The stiffness against horizontal bending as an RC section with tension reinforcement only by using the effective cross-sectional area converted from the tensile stiffness of the interlocking joint. The relationship of strength and converted plate thickness of the interlocking jopint is shown in **Fig. 13**. The following relationship is regressively obtained between the tensile strength and equivarent plate thickness of interlocking joint from the test results:

$$T_u / f_{sy} = 1.0385 \times 10^3 \, t_j$$

where,

T_u: Tensile strength of interlocking joint per unit length (N/m)

f_{sy}: Yield tensile stress of steel composing C-joint (N/mm^2)

t_j: Plate thickness of interlocking joint with equivalent tensile stiffness per unit length (mm)

The stiffness when bent in horizontal direction in allowable stress design is derived by obtaining the equivalent cross-sectional area of steel by the following equation and calculating the RC cross section:

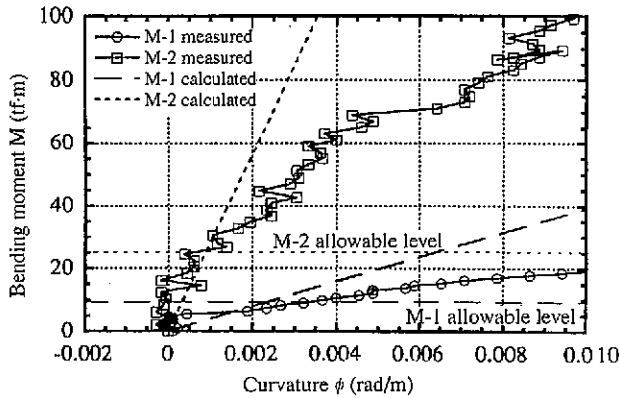$$t_j = T_a / 5.885 \times 10^2 f_{sa}$$

where,

T_a (= T_u / 3): Allowable tensile strength of interlocking joint per unit length (N/m)

f_{sa} (= f_{sy} / 1.7): Allowable tensile stress of steel composing C-joint (N/mm^2)

2.2.3 Confirmation of horizontal shear performance and establishment of shear design method

The shear load-bearing mechanism in horizontal direction in a steel diaphragm wall may be evaluated by regarding the steel diaphragm wall as a steel-concrete sandwich structure in which a steel shell is composed of flanges with an interlocking joint at each end, and webs, and is filled with concrete. The members were tested for horizontal shear performance using specimens shown in **Figs. 14 and 15**. The "Guidelines for Design of Steel-Concrete Sandwich Structures (Draft)" of the Japan Society of Civil Engineers was studied for its applicability to this structure.

The load–displacement curves are shown in **Fig. 16**. Each speci-

Width of 600 mm. MS-2 joints are made of 12-mm thick steel plate

Fig. 14 Schematic illustration of specimens MS-1 and MS-2

Width of 600 mm. S-2 joints are made of 12-mm thick steel plate

Fig. 15 Schematic illustration of specimens S-1 and S-2

Fig. 12 Relationship between bending moment and curvature

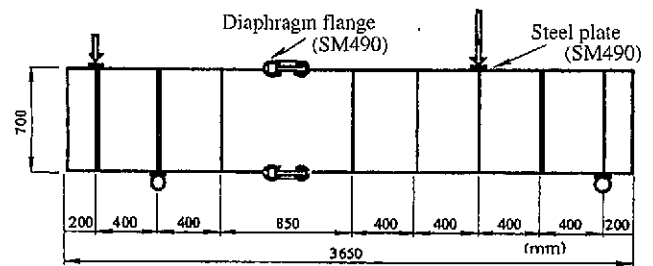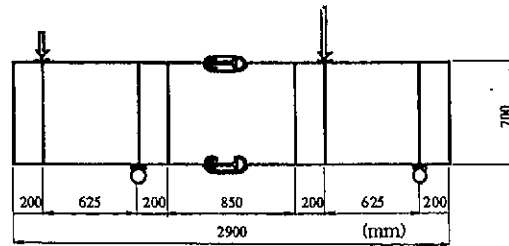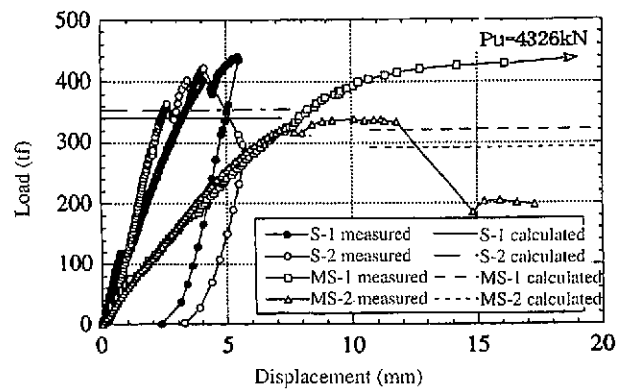**Fig. 13 Relationship between strength and equivalent plate thickness of interlocking joints**

Fig. 16 Load–displacement curves of horizontal shear test specimens

men had diagonal concrete cracks at flange–web junction, and reached the ultimate state upon the yielding of the corner flanges or the fracture of the concrete. The test results are listed in **Table 5**. The maximum test load exceeded the load values calculated according to the guidelines mentioned above by about 10 to 40%. The principal stresses of the concrete are shown in **Fig. 17**, and the relationship between the load and the tensile force of the flange and web is shown in **Fig. 18**. The principal compressive strain of the filled concrete just before reaching ultimate state formed diagonally with a spindle-like distribution. The calculated values of axial force converted from the flange and web steel strains agree well with the calculated values of the steel-concrete sandwich structure assumed as a truss mechanism.

These observations indicate that the shear load-bearing mechanism of the horizontal members in the steel diaphragm wall can be explained by applying the above-mentioned guidelines and that

Fig. 18 Relationship between load and axial force of flange and web

the shear capacity of the horizontal members can be evaluated conservatively by calculating with the equations given in the guidelines. To ensure the versatility of the shear design of horizontal steel diaphragm wall members, these equations were rewritten from the ultimate state design method to the allowable stress design method by providing a safety factor equivalent to that described in the "Standard Specification for Design and Construction of Concrete Structures" of the Japan Society of Civil Engineers, which is based on the above-mentioned guidelines. Namely, the allowable shear stress of the concrete was defined as τ_{aa} so that the diagonal concrete crack fracture strength $(0.188 \sqrt{f'_{cd}} \, \beta_d \, \beta_p \, \beta_s)$ would have a safety factor of 2.61 to 2.92, which is equivalent to that of τ_{a2} described in the Standard Specification for Design and Construction of Concrete Structures (see **Table 6**). That is, τ_{aa} can be defined as follows:

$$\tau_{aa} = \left(0.188 \sqrt{f'_{cd}} \, \beta_d \, \beta_p \, \beta_s\right) / \left(1.25 \sqrt{f'_{cd}} / \tau_{a2}\right)$$
$$= 0.15 \, \beta_d \, \beta_p \, \beta_s \, \tau_{a2}$$

where,

τ_{aa}: Allowable shear stress when concrete fails by diagonal cracking (N/mm²)

τ_{a2}: Upper limit of allowable shear stress when diagonal tension reinforcement is calculated (N/mm²)

f'_{cd}: Design compressive strength of concrete (N/mm²)

$\beta_d, \beta_p, \beta_s$: Coefficients to obtain shear fracture strength of concrete

If the shear stress of the concrete may be required to exceed the allowable shear stress τ_{aa}, tie bars or webs can be attached to increase the yield strength of the concrete. When tie bars or webs are added, the allowable shear stress of the concrete can be increased according to the full-size test results of shear reinforcement. These measures help to cope with the corners of rectangular shafts and similar areas where the section force is predominant (see **Fig. 19**).

2.3 Construction results and future development

Since the Steel Diaphragm Wall Association was founded in

Table 5 Shear test results

Test case	Joint specification	Concrete compressive strength f_c (N/mm²)	Shear fracture load (kN) Measured value ①	Shear fracture load (kN) Calculated value ②	① ②
S-1	1,717kN/m	29	4,316	3,345	1.29
S-2	12-mm thick steel plate	31	4,130	3,463	1.19
MS-1	3,188kN/m	25	4,326	3,159	1.37
MS-2	12-mm thick steel plate	21	3,316	2,865	1.16

For S-1 joints, t_p = 16 (SM490), and T-joints B were used.
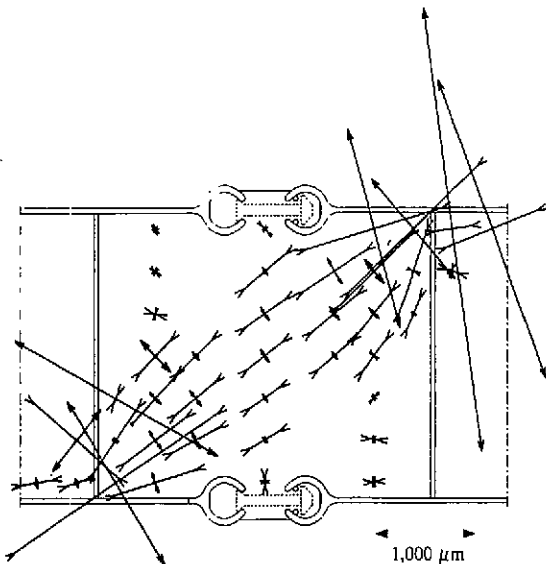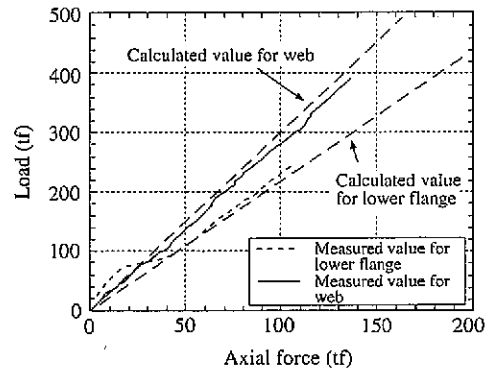For MS-1 joints, t_p = 16 (SM490), and T-joints B reinforced with hexagonal bars were used.

Fig. 17 Principal strain in concrete (MS-1: P = 4,326 kN)

1,000 μm

Table 6 Relationship between 1.25 $\sqrt{f'_{cd}}$ and τ_{a2} in standard specification for design and construction of concrete structures (N/mm²)

Characteristic strength of concrete, f_{ck}	18	20	24	26	29	34	39
Design compressive strength of concrete, f_{cd}	14	15	18	20	23	26	30
Allowable shear stress for calculation of diagonal tensile reinforcement, τ_{a2}	1.8	1.9	2.0	2.1	2.2	2.3	2.4
Diagonal compressive fracture strength of web concrete, 1.25 $\sqrt{f'_{cd}}$	4.7	4.8	5.3	5.6	6.0	6.4	6.8
$\kappa = 1.25 \sqrt{f'_{cd}} / \tau_{a2}$	2.61	2.53	2.65	2.67	2.73	2.78	2.83

(a) No special shear reinforcement   (b) Shear reinforcement with tie bars   (c) Shear reinforcement with webs
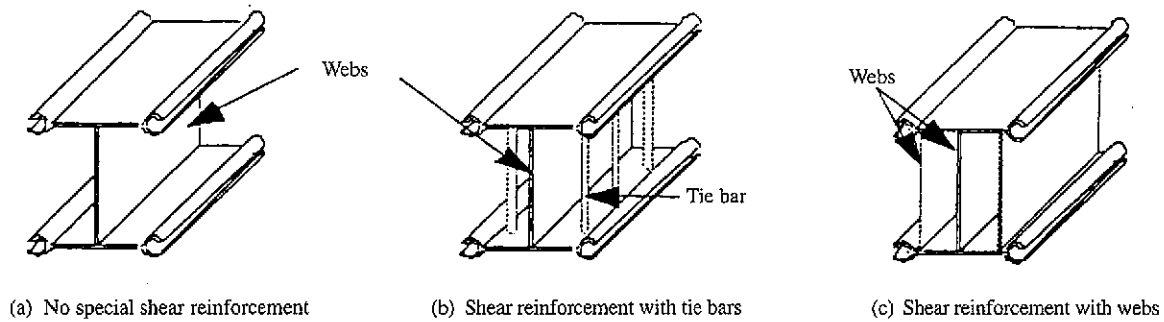
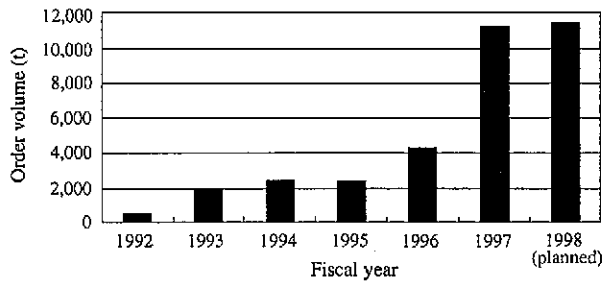Fig. 19 Shear reinforcement with tie bars and webs

Fig. 20 NS-BOX order volume

1992 (presently with 34 member companies), the demand for the steel diaphragm wall method using the GH type NS-BOX has rapidly increased (see **Fig. 20**). Main applications include tunnel advancing and arriving shafts, underground roads, and underground rail stations. Permanent structures accounted for 75% of these subterranean projects. The projects ranged from 15 to 92 m in construction depth, and 55% of them were 40 m or deeper. Main construction conditions are shown in **Photo 4.**

Given the possibility of reduced spending in future public works projects and the import of environmental issues, we are improving on the steel diaphragm wall method to lower the cost of construction, reduce the volume of industrial waste generated, and expand applications.

3. Concrete-Packed Steel Segments

When the primary lining of a shield tunnel is the principal structure member, the secondary lining serves to correct the meandering of the tunnel and to prevent vibration. It greatly affects long-term durability, including corrosion pretension, water tightness, and interior finish. The secondary lining is also considered to be effective in reinforcing the primary lining (segments). This reinforcement effect is especially important when the primary lining consists of steel segments. Coupled with recent improvements in lining analysis technology and accuracy, accurate load measurement, and enhancement of construction accuracy, there have appeared moves to review the role of the secondary lining. CP steel segments were developed to eliminate the secondary lining by providing the primary lining with the functions of the secondary lining, to reduce the tunnel outside diameter, and to lower the tunnel construction cost.

3.1 Concept of CP steel segments

The CP steel segment has concrete set in the steel shell of a steel segment at the factory (see **Fig. 21**). In terms of appearance, the inside surface is a concrete surface, and the remaining five
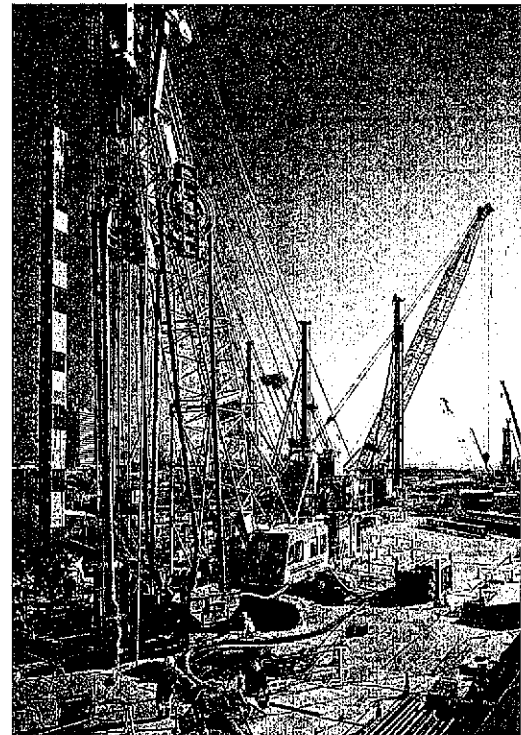
Erection of NS-BOX
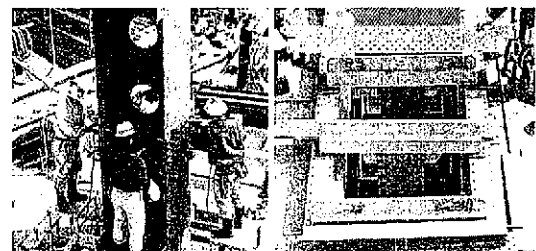
Joint bolting at site   Temporary supporting

Photo 4 MM21 Takashima Station construction site

surfaces (circumferential main beams, end flanges, and skin plates) are steel surfaces.

3.2 Advantages of CP steel segment application

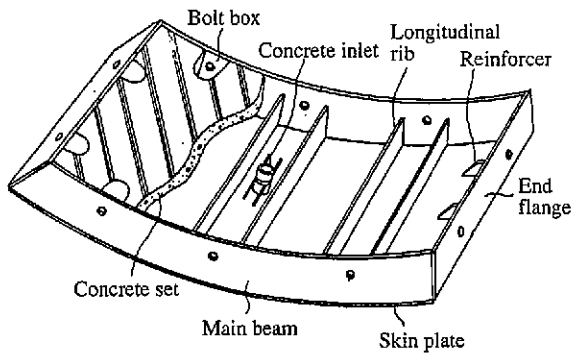The application of CP steel segments aims to provide the following advantages:

Fig. 21 Schematic illustration of concrete-packed steel segment

(1) Compared to steel segments, the lining thickness can be reduced, thus reducing the tunnel outside diameter.

(2) The coverage of the segment with a steel shell ensures the watertightness of the lining and prevents concrete chipping and cracking during construction.

(3) The filled concrete protects the inside of the steel shell from corrosion.

(4) The filled concrete carries the jack thrust of the shield machine to eliminate the need for the longitudinal ribs peculiar to steel segments and to reduce the steel weight.

(5) The CP steel segments are, in fact, prefabricated secondary lining pieces, and this helps to shorten the tunnel construction period.

3.3 Strength properties of CP steel segments

The results of bend testing conducted to determine the bending strength properties of the CP steel segments are shown in **Fig. 22**. The specimens were type A pieces, six of which comprised a ring. The outside diameter was 4,200 mm, the width B was 1,200 mm, the circumferential main beam height h was 145 mm, and the circumferential main beam thickness t was 12 mm. The design strength of the filled concrete is $\sigma_{ck} = 28$ kN/cm^2.

The concrete in the steel shell and the steel shell itself act together like a composite structure, as shown in **Fig. 22**. If the design method as the composite structure is established to make
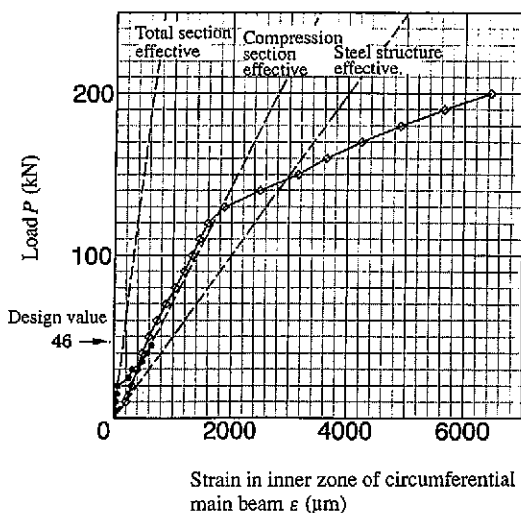
good use of its performance properties, the design method as the composite structure will be more rational.

3.4 Inner water pressure-resistant CP steel segments

CP steel segments with four circumferential main beams were developed for use in tunnels in which the segment joints are subjected to tensile forces resulting from high inner water pressure or unbalanced loads. This inner water pressure-resistant CP steel segment is illustrated in **Figs. 23** and **24**. It is structurally characterized by long bolts that secure inner circumferential main beams between rings. The axial forces in the tunnel are transferred by these bolts and by the reinforcements connecting the inner circumferential main beams. The segments are joined by connecting the outer and inner circumferential main beams with high-stiffness members like square steel bars. These high-stiffness members are then fastened with bolts, so that the bolt tension forces are transmitted directly to the circumferential main beams, not through the end flanges. These structural measures provide high-stiffness joint performance without what is called lever reaction force.

3.5 Strength properties of inner water pressure-resistant CP steel segments

Segments, six per ring and with an outside diameter of 4,500 mm, width of 1,200 mm, thickness of 150 mm, and four circumferential main beams each, were designed, fabricated, and tested to determine their structural performance properties.

3.5.1 Simple bending test

Each specimen had four circumferential main beams of 16-mm thickness, and the design strength σ_{ck} of the filled concrete was 28 kN/mm^2.

The strength and stiffness were both formed to be those of a composite structure (see **Fig. 25** and **Photo 5**).
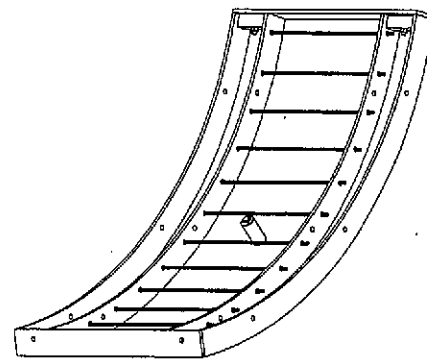

Fig. 23 Schematic illustration of steel shell

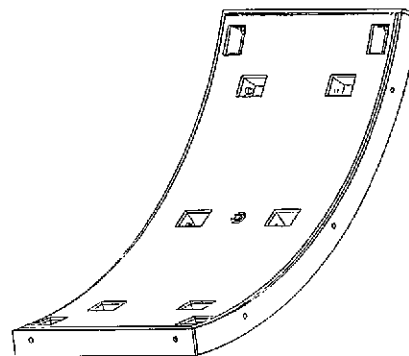Fig. 22 Load–strain curves in single bending test
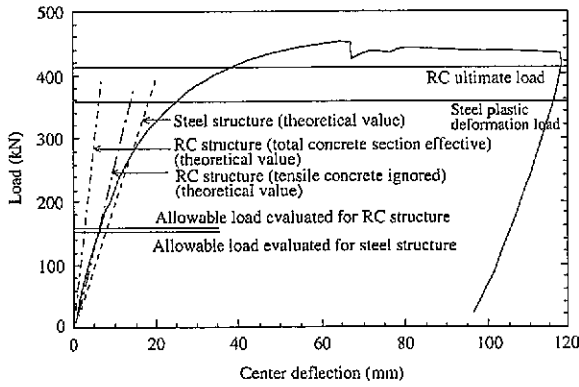

Fig. 24 Schematic illustration of product

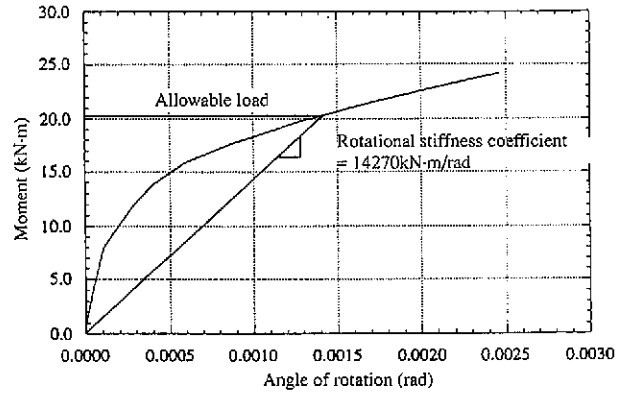Fig. 25 Load-deflection curves in single bending test

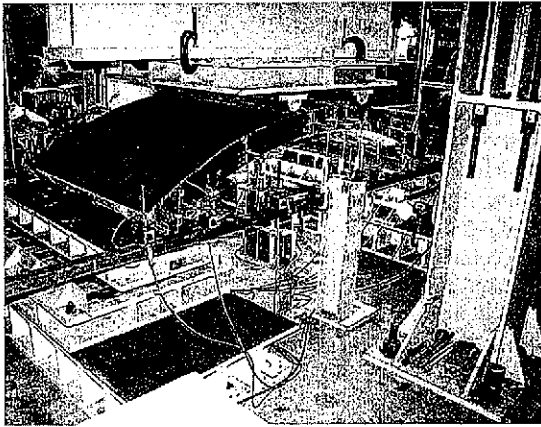Fig. 26 Relationship between moment and angle of rotation

Photo 5 Specimen in single bending test

3.5.2 Joint bending test

Joints were bend tested to learn their structural properties. Each specimen had two outer circumferential main beams of 12-mm thickness and two inner circumferential main beams of 25 mm thickness. The design strength σ_{ck} of the filled concrete was 30 kN/mm². The joint stiffness was as high as initially expected. The nondimensional coefficient of rotational stiffness used to evaluate the joint stiffness was a high 6.1. The joints opened almost uniformly and indicated no effect of lever reaction force (see Figs. 26 and 27, and Photo 6).

3.6 Long-term durability of inner water pressure-resistant CP steel segments

The filled concrete in the CP steel segments protects the steel shell from corrosion as previously described. If water is to flow through the tunnel, for example, the steel shell can be coated with a heavy-duty paint or special coating to ensure even greater protection against corrosion. The filled concrete may be changed to a type that offers higher durability. In short, the CP steel segments can be designed and made to meet a variety of needs.

3.7 Future development of CP steel segments

We will further improve secondary lining functions of the CP steel segments, increase the functionality of shield tunnel segments, and decrease their cost.
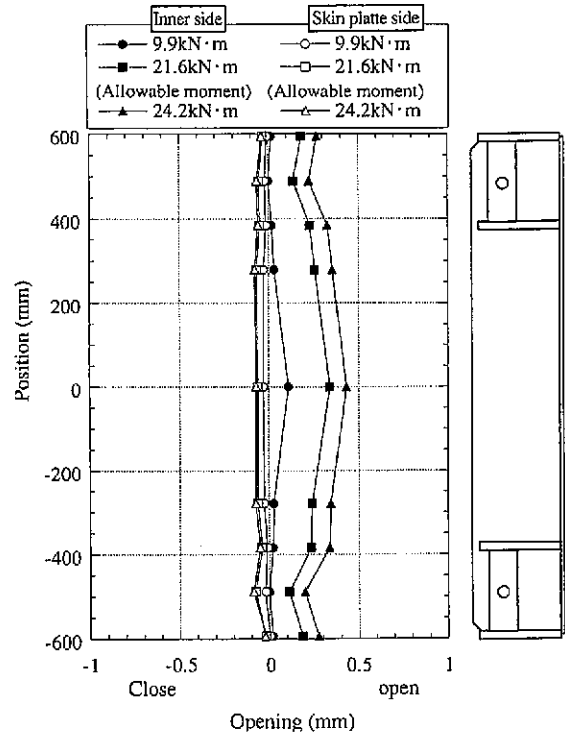

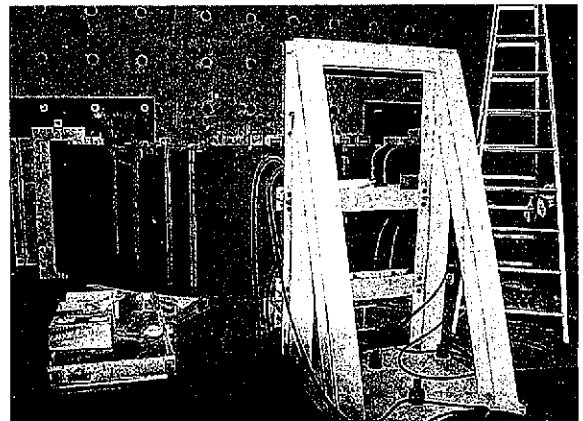Fig. 27 Joint opening measurement

Photo 6 Joints in bending test

4. High-Stiffness Joints (High-Performance Segment Joints)

4.1 General

The joints used to assemble segments into rings account for about 10 to 20% of the total segment fabrication cost. Joint optimization and joint cost reduction are critical in lowering the construction cost of shield tunnels. The remarkable progress of shield tunneling technology has increased the construction of large-diameter subway tunnels, internal pressure-type underground river tunnels, and many other shield tunnels in the soft ground in which joints are subjected to large sectional forces. These tunnels call for the use of segment joints with even higher stiffness and strength.

To meet this need, we have developed high-stiffness joints which are both low-cost and high performance as segment joints. The high-stiffness joints are ductile cast iron segment joints that provide high stiffness and strength despite their small thickness and weight by means of a three-dimensional tied arch structure in the form of a hollow dome (see **Fig. 28**).

4.2 Principle and features of high-stiffness joints

The stiffness and strength of segment joints are generally much lower than those of the segments themselves. If segments are assembled with weak joints, the resultant rings may lack in strength and cut-off performance. Moreover, the possible excessive deformation of the rings may have an adverse effect on ring assembly and ground subsidence. This is especially true when the tunnel is driven through soft ground or subjected to inner water pressure, and large bending moments or tensile forces act on the segment joints. In such a case, the stiffness of the entire ring must be assured by a joint structure with high stiffness.

The high-stiffness joints can smoothly transfer the axial force of the bolts through the arch to the anchor bars and thus can keep the deformation of the joint plates to a minimum. For this reason, joint stiffness and strength can be both improved by about 40 to 50% compared with conventional joints which may cause the joint plates to deform at a relatively low load level due to stress concentration around bolt holes (see **Fig. 29**).

The high-stiffness joints have the following features:

1) High stiffness and strength can be assured despite small thickness and weight.

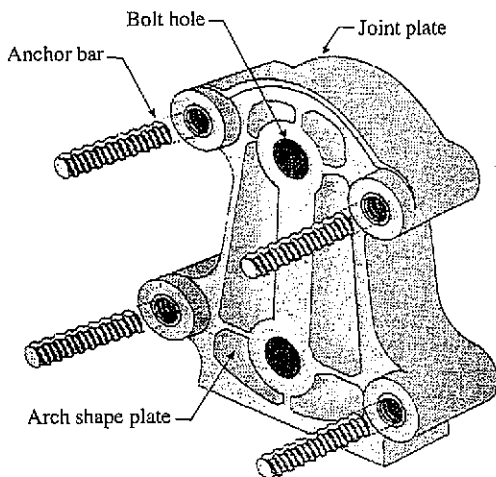Since the axial force of the bolts is transferred from the arch

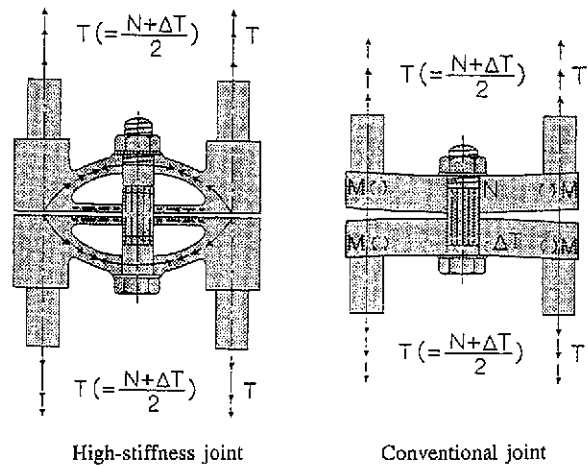High-stiffness joint   Conventional joint

Fig. 29 Deformation behavior of high-stiffness joint as compared with conventional joint

directly to the anchor bars, the joints have high stiffness and strength, although they are hollow and small in thickness and weight.

2) The segment structure can be optimized.

The high stiffness of the joints allows the sectional force applied to the splice rings to be reduced in the design stage. This helps to reduce the sectional force applied to the segments and to optimize the segment structure.

3) Excellent cut-off performance can be assured.

When external forces (bending moments) act on the joints and significantly deform the joint plates, the joints open widely causing water leakage. The high-stiffness joints undergo a very small deformation of this type and minimize the likelihood of water leakage.

As mentioned above, the high-stiffness joints feature excellent cost and performance. Their properties become more noteworthy when they are subjected to larger sectional forces.

4.3 Development of high-stiffness joint design model

The three-dimensional tied arch structure of the high-stiffness joints is its greatest advantage in terms of strength performance, but was difficult to model and called for advanced analytical computation in the design phase. We developed a simple and versatile design model to optimize the design of the high-stiffness joints.

The representation of the complicated three-dimensional tied arch structure by a simple, abstract model was the greatest achievement in the development of the design model. Model analysis that faithfully reproduced the actual structure was carried out to identify the strength properties of the high-stiffness joints. The strength properties were then abstracted to build a design model for the high-stiffness joints. The three-dimensional finite element analysis performed to identify the strength properties of the high-stiffness joints and the design model built on the basis of the results of that analysis are described below.

First, the analytical model used to analyze the force transfer mechanism is shown in **Fig. 30**, and the analytical results are given in **Fig. 31**. The analysis is concerned with the stress distribution of the joint when the concentrated load is applied to the bolt portion from above, on the joint's Z-axis. Our initial expectations were confirmed: the high-stiffness joints transmit the axial forces of the bolts through the arch to the anchor bars without stress concentration around the bolt holes.
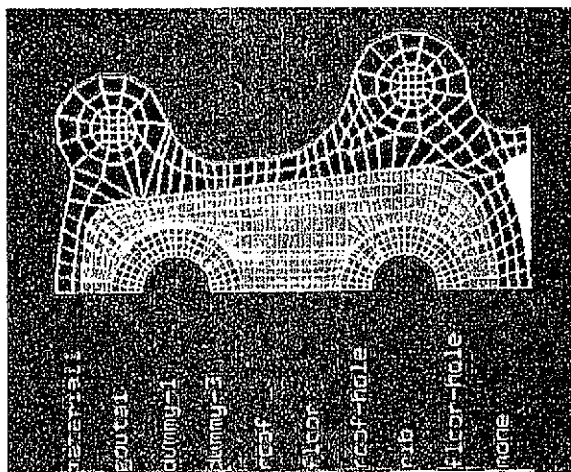

Bolt hole
Anchor bar
Joint plate
Arch shape plate

Fig. 28 Schematic illustration of high-stiffness joint

Fig. 30 Force transfer mechanism analytical model
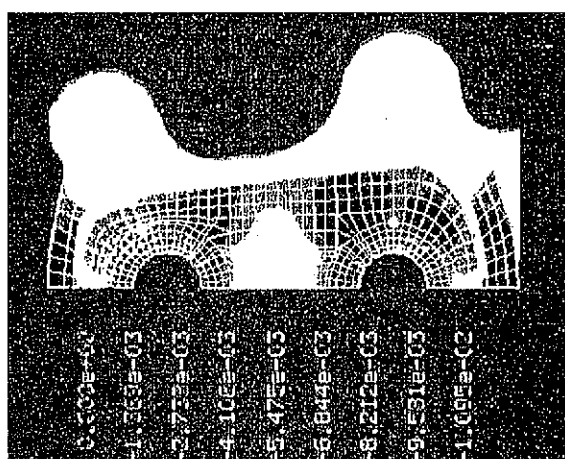
Fig. 31 Force transfer mechanism analytical results

Fig. 32 Deformation behavior analytical model

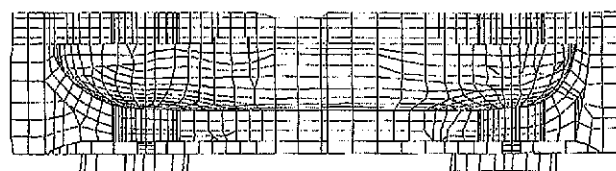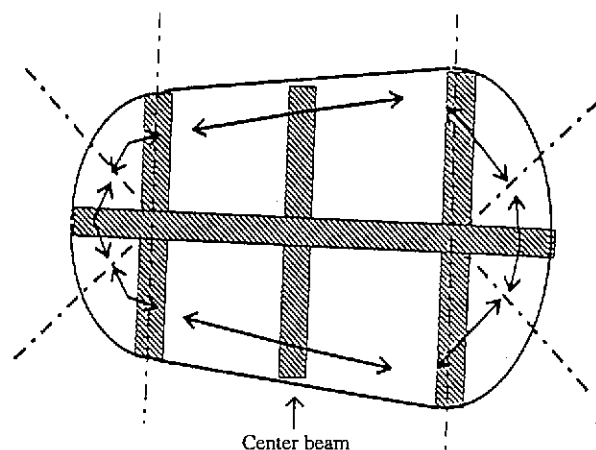Fig. 33 Deformation behavior analytical results (positive bending)

Fig. 34 Design model
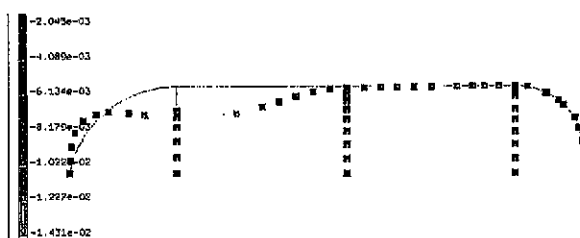

Fig. 35 Analytical results (positive bending)

Next, the analytical model used for analyzing the deformation behavior of the joints due to external forces is shown in **Fig. 32**, and the analytical results are given in **Fig. 33**. The analysis assumed the application of bending moment to the joint and revealed the deformation behavior of the joint when the load was applied to only one of the two bolts. It was confirmed that joint deformation was limited to only one side, and on the Y-axis.

The design model (three-dimensional beam model) created on the basis of these analytical results is shown in **Fig. 34**. The center beam in the model shows that the influence range of the joint deformation in finite element analysis is confined near the center point on the Y-axis. The deformation of the high-stiffness joint due to external force as simulated by the model is shown in **Fig. 35**. The simulation results agreed well with the results of the three-dimensional finite element analysis and verified the validity of the high-stiffness joint design model.

These findings indicate that the high-stiffness joints can be designed by a simple model, rather than a complex, three-dimensional finite element model. This design theory will be programmed into a general-purpose design system for more optimally designing the high-stiffness joints.

4.4 Application results of high-stiffness joints

The high-stiffness joints are effective in large-diameter shield tunnels in soft ground and shield tunnels subjected to internal pressures (see **Fig. 36**). When high-stiffness joints of the insert type or high-stiffness joints with bolt holes drilled in steel reinforcements are used, further cost savings can be achieved for some types of tunnels. For a sample calculation, insert-type high-stiffness joints
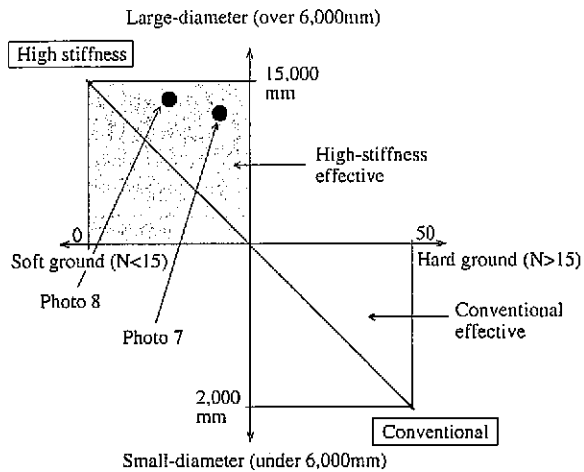
Large-diameter (over 6,000mm)

High stiffness

15,000 mm

High-stiffness effective

0

50

Soft ground (N<15)

Hard ground (N>15)

Photo 8

Conventional effective

Photo 7

2,000 mm

Conventional

Small-diameter (under 6,000mm)

Fig. 36 Competitiveness of high-stiffness joint as compared with conventional joint

were found to be capable of reducing the segment joint and segment fabrication costs by about 40 and 7%, respectively, compared with conventional joints.

For such reasons, the usage of high-stiffness joints has steadily grown and reached a total of nearly 10,000 tons (see **Table 7**, and **Photos 7** and **8**).

We will make further improvements to the design, manufacture and fabrication technology of the high-stiffness joints with the aim of reducing the construction cost of shield tunnels in a wider spectrum of applications.

Table 7 Application results of high-stiffness joints in main tunnel projects

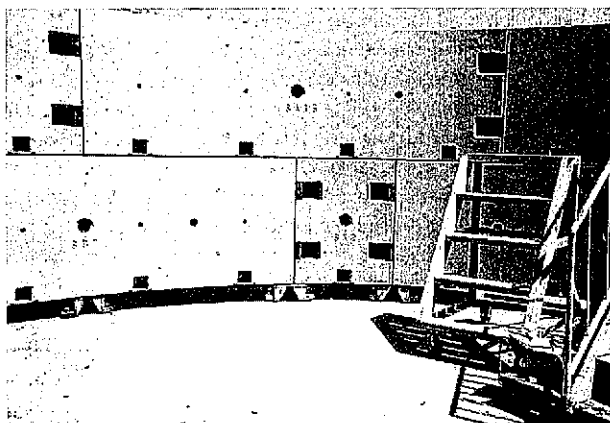|	Quantity (t)	Main project	Remarks
Underground river tunnels	6,100	Outer Metropolitan Diversion Tunnel	High-stiffness joints
Subway tunnels	3,100	Saitama Railway Line	Insert-type high-stiffness joints
Utility tunnels	150	Kawagoe Utility Tunnel	Insert-type high-stiffness joints

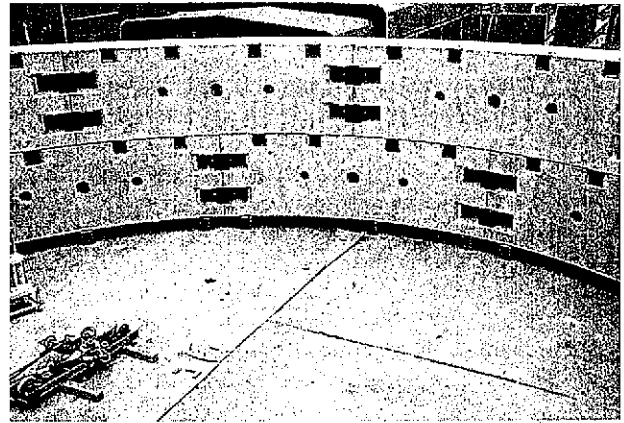**Photo 7 Application example of insert-type high-stiffness joints in subway tunnel**

Photo 8 Application example of connection-type high-stiffness joints in underground river tunnel

5. Conclusions

Although the need for construction in underground space has temporarily stagnated since the collapse of Japan's bubble economy, such construction is indispensable for the future growth of urban areas. The steel diaphragm wall members (NS-BOX), CP steel segments, and high-stiffness segment joints described in this paper are receiving acclaim in their respective fields of application and are considered to contribute greatly to the acceleration of deep underground space utilization.